Time Domain Simulation of (Resonance) Raman Spectra of Liquids in the Short Time Approximation

Mattiat, Johann ; Luber, Sandra

Abstract: Real-time time-dependent density functional theory (RT-TDDFT) and ab initio molecular dynamics (AIMD) are combined to calculate non-resonant and resonant Raman scattering cross sections of periodic systems, allowing for an explicit quantum mechanical description of condensed phase systems and environmental effects. It is shown that this approach to Raman spectroscopy corresponds to a short time approximation of Heller's time-dependent formalism for the description of Raman scattering. Two ways to calculate the frequency-dependent polarizability in a periodic system are presented: (1) via the modern theory of polarization (Berry phase) and (2) via the velocity representation. Both approaches are found to be equivalent for a system of liquid (S)-methyloxirane with the computational settings used. Resulting non-resonance and resonance Raman spectra from the dynamic AIMD/RT-TDDFT approach are compared to the spectra of one gas phase molecule in the harmonic approximation highlighting finite temperature and solvation effects. Using RT-TDDFT to calculate the full frequency-dependent Placzek-type polarizability within one set of simulations covers the non-resonance, near-resonance, and on-resonance regimes on equal footing, thus allowing the calculation of full Raman excitation profiles.

DOI: https://doi.org/10.1021/acs.jctc.0c00755

Time domain simulation of (resonance) Raman spectra of liquids in the short time approximation

J. Mattiat and S. Luber*

Department of Chemistry, University of Zurich, Zurich, Switzerland

E-mail: sandra.luber@chem.uzh.ch

Abstract

Real-time density functional theory (RT-TDDFT) and ab initio molecular dynamics (AIMD) are combined to calculate non-resonant and resonant Raman scattering cross sections for periodic systems, allowing for an explicit quantum mechanical description of condensed phase systems and environmental effects. It is shown that this approach to Raman spectroscopy corresponds to a short time approximation of Heller's time-dependent formalism for the description of Raman scattering. Two ways to calculate the frequency dependent polarizability in a periodic system are presented: 1. Via the modern theory of polarization (Berry phase). 2. Via the velocity representation. Both approaches are found to be equivalent for a system of liquid (S)-methyloxirane with the computational settings used. Resulting non-resonance and resonance Raman spectra from the dynamic AIMD/RT-TDDFT approach are compared to the spectra of one gas phase molecule in the harmonic approximation highlighting finite temperature and solvation effects. The use of RT-TDDFT to calculate the full frequency dependent Placzek type polarizability within one set of simulations covers the non-resonance, near-resonance and on-resonance regimes on equal footing, thus allowing the calculation of full Raman excitation profiles.

1 Introduction

Since its prediction and discovery the Raman effect has been a valuable tool in order to advance our understanding of matter and is today used in many flavours and variations across a variety of disciplines. Examples include but are not limited to proteins,[1] lipids,[2] and the characterization of novel materials.[3,4] The advancement of experimental techniques includes coherent anti-Stokes Raman scattering (CARS),[5] surface enhanced Raman spectroscopy (SERS),[6,7] tip-enhanced Raman spectroscopy (TERS)[8] and many more. The development of new techniques aims at enhancing the Raman signal either by increasing the strength of the electro-magnetic field, as e. g. in SERS or TERS, or exciting the system near or at an electronic resonance, or both. These developments make it desirable to have a theoretical framework to predict non-resonance as well as resonance Raman spectra from ab initio calculations.

Although a general description of a two photon process was given by Kramers and Heisenberg[9] and Dirac, Fowler and Bohr[10,11] already almost 100 years ago, routine calculations of resonance Raman (RR) scattering cross sections were out of reach, due to the more involved description of the coupling of nuclear and electronic degrees of freedom (vibronic coupling). However, Placzek gave a limiting expression for the Raman scattering cross section in the non-resonant Raman (NR) case in 1933, which proved to be very useful for the simulation of NR scattering. Three decades later an applicable theory for the description of RR scattering was put forth by Albrecht,[12] where a perturbative expansion of the electric transition dipole moments in the nuclear coordinates is used in the original expression by Kramers, Heisenberg and Dirac (KHD). However this formulation requires the calculation of sum over states expressions. Complementary to this perturbative approach in the frequency domain Lee and Heller provided a description of RR scattering in the time domain,[13] where the scattering cross section is expressed in terms of wave packet correlation functions. A useful semi-classical approximation of this theory is the so-called short time approximation (STA) which considers only the wave packet dynamics around the Franck-Condon point.[14] A recent

comparison between Albrecht's theory and the STA is given in Ref.[15]

Concerning practical calculations of RR scattering cross sections, the prohibitive cost of the application of Albrecht's theory can be overcome by transform theory,[16–18] using Kramers–Kronig relations of the experimental absorption spectrum. With the development of faster computers and modern quantum chemistry codes, Albrecht's theory,[19,20] a harmonic approximation of Heller's approach,[21] as well as the STA[22,23] were made available within a linear response (LR) time-dependent (TD) density functional theory (DFT) framework. Various simulations of RR scattering amplitudes include transition metal complexes,[21,24–28] the simulation of SERS,[29,30] diradicals and dye molecules,[31,32] among others.

Efforts to simulate Raman scattering can be categorized broadly into static or dynamic approaches as well as their respective level of inclusion of the environment. Static calculations, which rely on geometry optimizations of the system of interest, assume a temperature of 0 K and are usually carried out in the harmonic approximation.[33] Intensity-tracking has been used to selectively converge certain bands of interest.[34] Recently an analytic scheme to also include anharmonic effects in the gas phase was presented using generalized vibrational second-order perturbation theory.[35] LR-TDDFT is widely used due to the good compromise between effort and accuracy. Equivalently real time (RT)-TDDFT can be employed which allows the calculation of off-, near- and on-resonance effects.[36,37] In static calculations, environmental effects may be included by adding a few solvent molecules in the simulation[22] or a non-quantum mechanical approximation of the environment using e. g. polarizable continuum models[19,38,39] or a QM/MM approach.[40,41]

Dynamic approaches for vibrational spectroscopy can be carried out e . g. in a DFT-based MD framework (usually referred to as ab initio MD (AIMD)) where the nuclei are moved classically on a potential energy surface generated by a quantum mechanical description of the electrons. Periodic boundary conditions are employed in order to gain a quantum mechanical description of both system and environment in the condensed phase, but also examples of dynamic gas phase Raman calculations have been described[42] as well as a com-

bination of MD with QM/MM[43] in order to investigate proteins. Within AIMD the NR scattering cross section is given by time autocorrelation functions of the Plazcek polarizability.[44–47] By their nature dynamic approaches go beyond the harmonic approximation and include finite temperature effects.

Considering the exceptionally wide range of research fields in which Raman scattering experiments are performed as well as the sufficient theoretical understanding and the computational power at hand, it is highly desirable to simulate (resonance) Raman experiments in a realistic way in order to gain understanding of the ongoing atomistic processes. As most experiments are usually performed in the condensed phase such as the liquid state there are two challenges to overcome: 1. An efficient description of near-resonance and on-resonance Raman scattering; and 2. A sufficient description of environment and the condensed phase in general beyond a gas phase / harmonic approximation picture.

Extending our previous work on NR AIMD calculations based on density functional perturbation theory (DFPT)[46] as well as static calculations of NR, near-resonance and RR spectra using RT-TDDFT,[37] a promising route to overcome these challenges is a combination of AIMD and RT-TDDFT. In this work we use two different approaches for the calculation of the electric dipole moments in a periodic simulation cell: On the one hand a Berry phase formula is used, which naturally describes the electronic polarization (dipole per unit length) in a periodic system. On the other hand, these results are compared to a description in the velocity representation. This is different to previous work[48] which relies on a division of electronic densities by Voronoi tesselation. As a sample system we used liquid S-methyloxirane as recently investigated by one of the authors for the simulation of NR scattering in an AIMD framework with DFPT,[46] which reduced the computational cost as the AIMD trajectory was readily available.

This work is structured as follows: In Sec. 2 a derivation of the scattering cross section for the combined MD and RT-TDDFT approach is given and shown to correspond to the short time approximation. The calculation of electric dipole moments in a periodic simulation

cell is discussed in short, including the case of non-local pseudo potentials which introduce an additional term for the velocity representation. Computational details are described in Sec. 3. In Sec. 4 resulting spectra are given for a gas phase (S)-methyloxirane molecule in the harmonic approximation and liquid phase (S)-methyloxirane calculated using the dynamic approach, combining RT-TDDFT and AIMD. After a discussion of their respective absorption spectra, first the gas phase NR and RR spectra are shown and discussed, including a qualitative analysis of the RR peaks for the first three electronic excitations. Second, the resulting NR and RR scattering cross sections of the liquid system are presented for two ways of calculating the electric dipole moment in a periodic simulation cell (Berry phase and velocity representation). Then the gas phase spectra are compared to the one of the liquid for the non-resonant and resonant case and finally a full Raman excitation profile for the liquid is presented. Conclusions and outlook are given in Sec. 5.

2 Theory

The differential scattering cross section for light-matter interaction as a two photon process is given by the Kramers–Heisenberg formula[9–11,49,50]

$$\frac{d\sigma}{d\Omega} = \sum_f \frac{\omega_I \omega_S^3}{(4\pi\epsilon_0)^2 c^4} |M|^2 \, \delta(E_i + \hbar\omega_I - E_f - \hbar\omega_S) \tag{1}$$

where ϵ_0 the permitivity of vacuum, $\hbar$ Planck's reduced constant and c the speed of light in vacuum. The δ-function ensures energy conservation between the incoming (annihilated) and scattered (created) photons with energies $\hbar\omega_I$ and $\hbar\omega_S$ respectively, and the initial and final energy levels E_i and E_f. The Raman shift $\hbar\tilde{\omega}$ is the energy difference between the incoming and scattered photon, respectively the initial and final energy levels of the system:

$$\hbar\omega_I - \hbar\omega_S = E_f - E_i \equiv \hbar\tilde{\omega}. \tag{2}$$

M in Eq. (1) is given as

$$M = \sum_l \left[\frac{(\vec{u}^S \vec{D}_{fl})(\vec{u}^I \vec{D}_{li})}{E_l - E_i - \hbar\omega_I - i\hbar\Gamma_l} + \frac{(\vec{u}^I \vec{D}_{fl})(\vec{u}^S \vec{D}_{li})}{E_l - E_i + \hbar\omega_S - i\hbar\Gamma_l} \right]. \tag{3}$$

$\vec{u}^I$ and $\vec{u}^S$ represent the unit polarization vectors of the incoming and scattered photon and $\vec{D}_{ab}$ a matrix element of the electric dipole moment operator

$$\vec{D}_{ab} = \langle a|\hat{\vec{d}}|b\rangle \, . \tag{4}$$

The electric dipole moment operator is defined as $\hat{\vec{d}} = \sum_i q_i \hat{\vec{r}}_i$ where the sum runs over all particles in the system and q_i denotes their charge. An energy eigen state with energy E_a is denoted as $|a\rangle$. $1/\Gamma_l$ is an ad-hoc lifetime of state $|l\rangle$ and the index l runs over all excited states of the molecular system. The same sign convention for the life time is adopted. $|i\rangle$ and $|f\rangle$ denote the initial and final states of the system under study.

Eq. (3) can also be written in a tensorial notation by rewriting the scalar products in the

nominator of the first term as

$$\left(u_\alpha^S \langle f|\hat{d}_\alpha|l\rangle\right)\left(\langle l|\hat{d}_\beta|i\rangle\, u_\beta^I\right) = u_\alpha^S\left(\langle f|\hat{d}_\alpha|l\rangle\ \langle l|\hat{d}_\beta|i\rangle\right)u_\beta^I \equiv u_\alpha^S\tilde{\alpha}_{\alpha\beta}^{fli}u_\beta^I \tag{5}$$

using Einstein's summation convention and α, β stand for the Cartesian room directions x, y, z. The second term of Eq. (3) leads to a similar expression: $u_\beta^I\tilde{\alpha}'^{fli}_{\beta\alpha}u_\alpha^S$. As the definition of M proceeds component-wise (scalar product) we may include the denominators and the sum over l, giving the two tensors, $\alpha_{\alpha\beta}^{fi}$ and $\alpha'^{fi}_{\beta\alpha}$. Pulling the polarization vectors $\vec{u}^I$ and $\vec{u}^S$ out of the sum gives $M \equiv u_\alpha^S\alpha_{\alpha\beta}^{fi}u_\beta^I + u_\beta^I\alpha'^{fi}_{\beta\alpha}u_\alpha^S$. As we will perform a rotational averaging later on this notation without explicitly writing the polarization vectors is convenient. The primed term $\alpha'^{fi}_{\beta\alpha}$ is often called non-resonant term as its value becomes negligible compared to the first term on resonance when its denominator $E_l - E_i \approx \hbar\omega_I$ approaches zero.

In the following we omit the indices i and f: $\alpha_{\alpha\beta}^{fi} \equiv \alpha_{\alpha\beta}$. $\alpha_{\alpha\beta}$ is commonly called (electric-dipole–electric-dipole) polarizability tensor. Both notations are employed in the remainder of this work.

In order to simplify Eq. (1) one often resorts to the Born–Oppenheimer (BO) approximation,[51] separating rotational, vibrational and electronic degrees of freedom of the molecular eigen state $|l\rangle = |n\rangle\,|v\rangle\,|r\rangle$. Here we do not consider the rotational states, as they are averaged out at a later stage. The polarizability tensor is then

$$\alpha_{\alpha\beta}^{\mathrm{KHD}} = \sum_{nv}\left[\frac{\langle f^0|D_{0n}^\alpha|v^n\rangle\,\langle v^n|D_{n0}^\beta|i^0\rangle}{E_{v^n} - E_{i^0} - \hbar\omega_I - i\hbar\Gamma_n} + \frac{\langle f^0|D_{0n}^\beta|v^n\rangle\,\langle v^n|D_{n0}^\alpha|i^0\rangle}{E_{v^n} - E_{i^0} + \hbar\omega_S - i\hbar\Gamma_n}\right] \tag{6}$$

where we changed the notation to the tensorial form and used a short-hand notation for the BO states: $|v^n\rangle$ denotes the vth vibrational state on the nth BO surface and E_{v^n} its energy. Eq. (6) is often referred to as Kramers–Heisenberg–Dirac (KHD) polarizability tensor. Note that $\vec{D}_{0n}$ is now an electronic transition dipole moment matrix element ($\vec{D}_{0n} = \langle 0|\hat{\vec{d}}|n\rangle$). We also assumed that both initial and final vibrational states belong to the electronic ground state BO surface.

The KHD polarizability tensor is e. g. the starting point for a time-dependent formulation of resonance Raman spectroscopy proposed by Heller et al.[13,14,52] which expresses the scattering amplitude for RR scattering in terms of correlation functions of wave packets[14]

$$M = \int_0^\infty \mathrm{d}t \ \left\langle \phi^f \middle| \phi^i(t) \right\rangle e^{i\tilde{\omega}_I t - \Gamma t} + \mathrm{NRT} \tag{7}$$

where $\tilde{\omega}_I = \omega_I + E_{i^0}/\hbar$, $\left|\phi^f\right\rangle = \vec{u}^S \vec{D}_{0n} \left|f^0\right\rangle$, $\left|\phi^i\right\rangle = \vec{u}^I \vec{D}_{0n} \left|i^0\right\rangle$ and $\left|\phi^i(t)\right\rangle = e^{-i\hat{H}_n t/\hbar} \left|\phi^i\right\rangle$, and $\hat{H}_n$ denotes the vibrational Hamiltonian for the excited nth BO surface. NRT stands for additional non-resonant terms. Thus, the RR scattering cross section is related to the overlap of the moving initial wave packet on the excited state surface with the final state.

A further simplification treats the vibrational degrees of freedom in a classical framework, following the original treatment of non-resonant Raman spectroscopy by Plazcek. The Plazcek polarizability depends parametrically on classical nuclear coordinates q:[53]

$$\alpha_{\alpha\beta}^{\mathrm{Plazcek}} = \alpha_{\alpha\beta}(\omega, q). \tag{8}$$

Accordingly the vibronic energies in the denominator of Eq. (6) are approximated by a parametric dependence on classical nuclear coordinates

$$E_{v^n} \cong E_n(q). \tag{9}$$

As shown by Lee[54] this treatment corresponds to a semi-classical STA of the KHD polarizability tensor, essentially neglecting the excited state dynamics and only considering the Franck–Condon point.[55] It can be rigorously derived by using the Wigner transform of the propagator in Eq. (7) and keeping only the first order term.[22,54] The resulting tensor is called Plazcek type polarizability (PtP) tensor[22]

$$\alpha_{\alpha\beta}^{\mathrm{PtP}}(\omega_I, q) = \sum_n \left[\frac{D_{0n}^\alpha D_{n0}^\beta}{E_n(q) - E_0(q) - \hbar\omega_I - i\hbar\Gamma} + \frac{D_{0n}^\beta D_{n0}^\alpha}{E_n(q) - E_0(q) + \hbar\omega_I - i\hbar\Gamma} \right] \tag{10}$$

where an average life time $1/\Gamma$ for the electronic states is assumed and we used $\omega_I \approx \omega_S$

in the second denominator. Due to the inclusion of the imaginary factor $i\hbar\Gamma$ this expression does not diverge in the resonant regime and therefore allows the description of resonant Raman scattering within the STA. As investigated in previous work by the authors[37] in the resonant case the STA is closely related the excited state gradient method,[14] as it is derived under the same assumptions. Note that the closure over the vibrational states is carried out here compared to Eq. (6). In effect, Eq. (10) corresponds to a classical treatment of nuclear motion and a quantum mechanical treatment of the electrons.

As $\omega_I \approx \omega_S$ if the energy of the exciting laser is sufficiently larger than the Raman shift we can write in Eq. (1)

$$\omega_I \omega_S^3 \approx \omega_S^4 = (\omega_I - \tilde{\omega})^4 \tag{11}$$

by virtue of Eq. (2).

Inserting Eq. (10) into Eq. (1) one arrives at the following approximation for the scattering cross section

$$\frac{d\sigma}{d\Omega} = \frac{(\omega_I - \tilde{\omega})^4}{(4\pi\epsilon_0)^2 c^4} \sum_f \left| \left\langle f^0 \middle| \vec{u}^S \boldsymbol{\alpha}^{\mathrm{PtP}}(\omega_I, q) \vec{u}^I \middle| i^0 \right\rangle \right|^2 \delta(\hbar\tilde{\omega} - E_{f^0} + E_{i^0}) \tag{12}$$

where only the sum over the final vibrational states remains and we have rewritten the energy conservation in the δ-function in terms of the Raman shift $\tilde{\omega} = \omega_I - \omega_S$ according to Eq. (2). Note that this notation implies neglecting the second term of Eq. (10) in the resonant case (at resonance the first term will be much larger due to the vanishing denominator) and taking the Placzek polarizability as limiting expression in the non resonant case.

For the sake of simplicity we drop the index 0 indicating the ground state potential energy surface and write $\omega_I = \omega$ in the following.

In the popular double harmonic approximation the PtP polarizability is expanded around the equilibrium geometry of the molecule in a Taylor expansion with respect to normal coordinates q_k:

$$\alpha_{\alpha\beta}(\omega, q) = \alpha_{\alpha\beta}(\omega, q_0) + \left(\frac{\partial \alpha_{\alpha\beta}(\omega, q)}{\partial q_k} \right)_{q=q_0} q_k + \ \cdots \tag{13}$$

The initial and final vibrational states $|i^0\rangle$ and $|f^0\rangle$ in Eq. (12) are taken to be eigen states of the harmonic oscillator corresponding to a specific normal coordinates q_k.[56] Then the first term of Eq. (13) relates to Rayleigh scattering, while the second term describes Raman scattering. In this semi-classical approach the Raman scattering cross section for a normal mode q is given as[56]

$$\frac{\mathrm{d}\sigma}{\mathrm{d}\Omega} = \frac{1}{(4\pi\epsilon_0)^2 c^4} (\omega - \tilde{\omega}_q)^4 \frac{\hbar}{2\omega_q} \frac{1}{1 - \exp[-\hbar\omega_q / k_B T]} S(a^2, \gamma^2) \tag{14}$$

where $\tilde{\omega}_q$ is the angular frequency of normal mode q, k_B the Boltzmann constant and T the temperature (it is most often quoted in terms of wave numbers $\tilde{\nu}$, which is obtained by substituting $\omega = 2\pi c\tilde{\nu}$). $S(a^2, \gamma^2)$ contains the isotropic and anisotropic invariants of α^{PtP} which arise from averaging over different orientations of the molecule.[53,57] The expression for S depends also on the experimental set-up.[58] For a scattering angle of $\frac{\pi}{2}$ and a linearly polarized incident beam with the electric field component perpendicular to the scattering plane, S is given as[53]

$$S(a^2, \gamma^2) = \frac{1}{45}(45a^2 + 7\gamma^2) \tag{15}$$

The isotropic and anisotropic invariants, a^2 and γ^2, are given as:

$$a^2 = \frac{1}{9} \mathrm{Re}\left[\alpha_{\alpha\alpha}\alpha^*_{\beta\beta}\right] = \frac{1}{9} \left|\mathrm{Tr}\left(\boldsymbol{\alpha}\right)\right|^2 = \frac{1}{9}|\alpha_{xx} + \alpha_{yy} + \alpha_{zz}|^2 \tag{16}$$

$$\begin{aligned} \gamma^2 &= \frac{1}{2} \mathrm{Re}\left[3\alpha_{\alpha\beta}\alpha^*_{\alpha\beta} - \alpha_{\alpha\alpha}\alpha^*_{\beta\beta}\right] \\ &= 3(|\alpha_{xy}|^2 + |\alpha_{yz}|^2 + |\alpha_{zx}|^2) + \frac{1}{2}(|\alpha_{xx} - \alpha_{yy}|^2 + |\alpha_{yy} - \alpha_{zz}|^2 + |\alpha_{zz} - \alpha_{xx}|^2) \end{aligned} \tag{17}$$

where the symmetry of the PtP polarizability tensor was considered. Note that within the approximations made in this work the polarizability tensor is always symmetric, although this is not generally the case for RR scattering.

For the dynamic framework beyond the harmonic approximation, it is convenient to convert Eq. (12) to the time domain, following Gordon[44,57,59] by representing the δ-function as an exponential

$$\delta(\hbar\tilde{\omega} - E_f + E_i) = \int_{-\infty}^{\infty} \mathrm{d}t \; e^{-i(\hbar\tilde{\omega} - E_f + E_i)/\hbar t} \tag{18}$$

giving

$$\frac{d\sigma}{d\Omega} = \frac{(\omega-\tilde{\omega})^4}{(4\pi\epsilon_0)^2 c^4} \int_{-\infty}^{\infty} \mathrm{d}t \; \sum_f \langle i|\vec{u}^S \boldsymbol{\alpha}^{\mathrm{PtP}}(\omega,q)\vec{u}^I|f\rangle \; \langle f|e^{iE_f t/\hbar}\vec{u}^S \boldsymbol{\alpha}^{\mathrm{PtP}}(\omega,q)\vec{u}^I e^{-iE_i t/\hbar}|i\rangle \, e^{-i\tilde{\omega}t}. \quad (19)$$

This formalism is easily extended to general mixed initial states writing[57]

$$\frac{d\sigma}{d\Omega} = \frac{(\omega-\tilde{\omega})^4}{(4\pi\epsilon_0)^2 c^4} \int_{-\infty}^{\infty} \mathrm{d}t \; \sum_f \sum_i \rho_i \, \langle i|\vec{u}^S \boldsymbol{\alpha}^{\mathrm{PtP}}(\omega,q)\vec{u}^I|f\rangle \; \langle f|e^{iE_f t/\hbar}\vec{u}^S \boldsymbol{\alpha}^{\mathrm{PtP}}(\omega,q)\vec{u}^I e^{-iE_i t/\hbar}|i\rangle \, e^{-i\tilde{\omega}t}. \quad (20)$$

where ρ_i denote the probability of occupying vibrational state $|i\rangle$.

Using the fact that the initial and final states, $|i\rangle$ and $|f\rangle$, are eigen states of the ground state vibrational Hamiltonian $\hat{H}_0$

$$e^{-iE_i t/\hbar}\,|i\rangle = e^{-i\hat{H}_0 t/\hbar}\,|i\rangle\,, \quad (21)$$

and the time evolution of an operator $\hat{O}$ in the Heisenberg picture is given by

$$\hat{O}(t) = e^{i\hat{H}_0 t/\hbar}\hat{O}e^{-i\hat{H}_0 t/\hbar}, \quad (22)$$

we can write

$$\frac{d\sigma}{d\Omega} = \frac{(\omega-\tilde{\omega})^4}{(4\pi\epsilon_0)^2 c^4} \int_{-\infty}^{\infty} \mathrm{d}t \; \sum_f \sum_i \rho_i \, \langle i|\vec{u}^S \boldsymbol{\alpha}^{\mathrm{PtP}}(\omega,q)\vec{u}^I|f\rangle \; \langle f|\vec{u}^S e^{i\hat{H}_0 t/\hbar}\boldsymbol{\alpha}^{\mathrm{PtP}}(\omega,q)e^{-i\hat{H}_0 t/\hbar}\vec{u}^I|i\rangle \, e^{-i\tilde{\omega}t}. \quad (23)$$

Carrying out the sum over the complete set of eigen states $|f\rangle$ one arrives at the following formula for the cross section

$$\frac{d\sigma}{d\Omega} = \frac{(\omega-\tilde{\omega})^4}{(4\pi\epsilon_0)^2 c^4} \int_{-\infty}^{\infty} \mathrm{d}t \; \sum_i \rho_i \, \langle i|\left\{\vec{u}^S \boldsymbol{\alpha}^{\mathrm{PtP}}(\omega,q)\vec{u}^I\right\}\left\{\vec{u}^S \boldsymbol{\alpha}^{\mathrm{PtP}}(\omega,q)(t)\vec{u}^I\right\}|i\rangle \; e^{-i\tilde{\omega}t}. \quad (24)$$

As $\boldsymbol{\alpha}^{\mathrm{PtP}}(\omega,q)$ is a classical operator with respect to the vibrational degrees of freedom, we

can write the time evolution as

$$\boldsymbol{\alpha}^{\mathrm{PtP}}(\omega, q)(t) = \boldsymbol{\alpha}^{\mathrm{PtP}}(\omega, q(t)). \tag{25}$$

Then Eq. (24) can be recast in terms of a classical auto correlation function

$$\frac{d\sigma}{d\Omega} = \frac{(\omega - \tilde{\omega})^4}{(4\pi\epsilon_0)^2 c^4} \int_{-\infty}^{\infty} \mathrm{d}t \left\langle \left\{ \vec{u}^S \boldsymbol{\alpha}^{\mathrm{PtP}}(\omega, q(0)) \vec{u}^I \right\} \left\{ \vec{u}^S \boldsymbol{\alpha}^{\mathrm{PtP}}(\omega, q(t)) \vec{u}^I \right\} \right\rangle \; e^{-i\tilde{\omega}t}. \tag{26}$$

Comparing to Gordon's original formulation which considered the non-resonant regime and therefore is often employed with static polarizabilities ($\omega \to 0$) only, in the approximation presented here the Plazcek type polarizability is explicitly frequency dependent and also involves the resonant regime within the STA. Essentially Eq. (26) represents a separate treatment of the electronic degrees of freedom via Eq. (10) and the vibrational degrees of freedom in a time domain fashion via a (classical) correlation function in Eq. (26). This is represented in the treatment of the vibrational degrees of freedom via AIMD and the treatment of the electronic degrees of freedom via the STA by means of RT-TDDFT.

Thus, using the PtP-polarizability auto-correlation formalism from Eq. (26), our working equations for the calculation of the invariants are

$$\begin{aligned} a^2 = \int \mathrm{d}t \; e^{-i\tilde{\omega}t} \Big\langle & \left[\alpha_{xx}^{\mathrm{PtP}}(\omega, q(0)) + \alpha_{yy}^{\mathrm{PtP}}(\omega, q(0)) + \alpha_{zz}^{\mathrm{PtP}}(\omega, q(0)) \right] \\ & \left[\alpha_{xx}^{\mathrm{PtP}}(\omega, q(t)) + \alpha_{yy}^{\mathrm{PtP}}(\omega, q(t)) + \alpha_{zz}^{\mathrm{PtP}}(\omega, q(t)) \right] \Big\rangle \end{aligned} \tag{27}$$

and

$$
\begin{aligned}
\gamma^2 = & \frac{1}{2}\int \mathrm{d}t\ e^{-i\tilde{\omega}t}\left\langle\left[\alpha_{xx}^{\mathrm{PtP}}(\omega,q(0)) - \alpha_{yy}^{\mathrm{PtP}}(\omega,q(0))\right]\left[\alpha_{xx}^{\mathrm{PtP}}(\omega,q(t)) - \alpha_{yy}^{\mathrm{PtP}}(\omega,q(t))\right]\right\rangle \\
& + \frac{1}{2}\int \mathrm{d}t\ e^{-i\tilde{\omega}t}\left\langle\left[\alpha_{yy}^{\mathrm{PtP}}(\omega,q(0)) - \alpha_{zz}^{\mathrm{PtP}}(\omega,q(0))\right]\left[\alpha_{yy}^{\mathrm{PtP}}(\omega,q(t)) - \alpha_{zz}^{\mathrm{PtP}}(\omega,q(t))\right]\right\rangle \\
& + \frac{1}{2}\int \mathrm{d}t\ e^{-i\tilde{\omega}t}\left\langle\left[\alpha_{zz}^{\mathrm{PtP}}(\omega,q(0)) - \alpha_{xx}^{\mathrm{PtP}}(\omega,q(0))\right]\left[\alpha_{zz}^{\mathrm{PtP}}(\omega,q(t)) - \alpha_{xx}^{\mathrm{PtP}}(\omega,q(t))\right]\right\rangle \\
& + 3\int \mathrm{d}t\ e^{-i\tilde{\omega}t}\left\langle\left[\alpha_{xy}^{\mathrm{PtP}}(\omega,q(0))\right]\left[\alpha_{xy}^{\mathrm{PtP}}(\omega,q(t))\right]\right\rangle \\
& + 3\int \mathrm{d}t\ e^{-i\tilde{\omega}t}\left\langle\left[\alpha_{yz}^{\mathrm{PtP}}(\omega,q(0))\right]\left[\alpha_{yz}^{\mathrm{PtP}}(\omega,q(t))\right]\right\rangle \\
& + 3\int \mathrm{d}t\ e^{-i\tilde{\omega}t}\left\langle\left[\alpha_{zx}^{\mathrm{PtP}}(\omega,q(0))\right]\left[\alpha_{zx}^{\mathrm{PtP}}(\omega,q(t))\right]\right\rangle
\end{aligned}
\tag{28}
$$

where the angular brackets denote the auto correlation function. As pointed out in Ref.[47] the auto correlation functions may also be calculated using the time derivatives of the polarizability tensor components, leading to an additional factor of $\tilde{\omega}^2$.

The scattering cross sections are then calculated according to

$$
\frac{d\sigma}{d\Omega} = \frac{1}{(4\pi\epsilon_0)^2 c^4}\frac{\hbar\tilde{\omega}/kT}{1-\exp(-\hbar\tilde{\omega}/kT)}(\omega-\tilde{\omega})^4 S(a^2,\gamma^2) \tag{29}
$$

where an additional quantum correction factor of $(\hbar\tilde{\omega}/kT)/(1-\exp(-\hbar\tilde{\omega}/kT))$ was used in order to correct for the classical treatment of nuclei.[60]

2.1 RT-TDDFT polarizability with periodic boundary conditions

In RT-TDDFT the time-dependent Kohn–Sham equations are integrated stepwise for small time steps and thus the time evolution of the electron density is constructed.[61] In order to obtain frequency dependent linear response functions, such as the PtP-polarizability, the linear response of the electric dipole moment to a field perturbation in the dipole approximation $\hat{\vec{d}}\cdot\vec{E}(t)$, where $\vec{E}(t) = \vec{\kappa}f(t)$, is tracked:

$$
\langle\hat{\vec{d}}(t)\rangle - \langle\hat{\vec{d}}\rangle_0 = \int_{-\infty}^{t}\mathrm{d}t'\ \boldsymbol{\alpha}(t-t')\vec{\kappa}f(t'). \tag{30}
$$

Here $\vec{\kappa}$ is the vector containing the field strength and direction while $f(t)$ gives the field's time evolution. This relation allows to calculate the frequency dependent PtP-polarizability via generalized Fourier transforms[62]

$$\alpha_{\alpha\beta}(\omega) = \langle \hat{d}_\alpha(\omega) \rangle / \left(\kappa_\beta f(\omega) \right) \tag{31}$$

where

$$\langle \hat{\vec{d}}(\omega) \rangle = \lim_{\epsilon \to 0^+} \int_{-\infty}^{\infty} \mathrm{d}t \, \left(\langle \hat{\vec{d}}(t) \rangle - \langle \hat{\vec{d}}(0) \rangle \right) e^{i\omega t} e^{-\epsilon t}. \tag{32}$$

ϵ is a damping factor which can be identified with the lifetime $1/\Gamma$ in Eq. (10) and is necessary for the calculation to converge. For a calculation of the full tensor in Eq. (31) three linearly independently polarized pulses have to be applied. It is convenient to apply a δ-pulse in order to excite all electronic transitions at once.[63]

In a periodic system the position operator and therefore the electric dipole moment are not well defined. Consequently only a change in polarization and not its absolute value is a meaningful concept. In this work, we will use two ways to obtain the electric-dipole–electric-dipole polarizability in a periodic system:

1. Modern theory of polarization (Berry phase)

2. Velocity representation of the polarizability

2.1.1 Berry phase formula

Building on the work of others,[64] Resta[65] and Vanderbilt[66] have developed the so-called modern theory of polarization realizing that the concept of a polarization in a periodic system is closely related to Berry phases. The main result is a periodic definition of the expectation value of the electric dipole operator, which is given for the Γ point of a cubic simulation cell for an insulator in a Kohn–Sham (KS) framework by

$$\langle \hat{d}_\alpha \rangle = f_{\mathrm{occ}} \frac{eL}{2\pi} \operatorname{Im} \ln \det S_\alpha \tag{33}$$

where L is the side length of the simulation cell, e the electric charge and f_{occ} the occupation number of the KS orbitals, assuming the same occupation number for all KS orbitals. The elements of S_α are given as

$$S_{\alpha,ij} = \left\langle \psi_i \middle| e^{-i\frac{2\pi}{L}\hat{r}_\alpha} \middle| \psi_j \right\rangle \tag{34}$$

where the ψ_i and ψ_j are KS orbitals. Substituting this expression in Eq. (32) allows for periodic calculations of the electric-dipole–electric-dipole polarizability.

2.1.2 Velocity representation

Instead of using the position operator the polarizability can also be obtained by employing the velocity operator, which is well defined in a periodic box as it is only concerned with the change of positions and not their absolute values. In RT-TDDFT this translates to tracking the velocity operator over time.[67,68]

In the presence of non-local potentials special care has to be taken to couple them correctly to the applied fields.[69–71] Essentially an additional commutator term between the non-local potentials and the position operator has to be taken into account:[67,68,72] For a Hamiltonian of the form $\hat{H}_0 = \frac{\hat{p}^2}{2m_e} + \hat{V}^{\text{loc}}(\vec{r}) + \hat{V}^{\text{nl}}$, including non-local as well as local potentials, its commutator with the position operator is

$$\left[\hat{\vec{r}}, \hat{H}_0\right] = \frac{i\hbar}{m_e}\hat{\vec{p}} + \left[\hat{\vec{r}}, \hat{V}^{\text{nl}}\right]. \tag{35}$$

$\hat{\vec{p}}$ is the canonical momentum operator. Thus, the electric transition dipole moment between two electronic energy eigen states $|a\rangle$ and $|b\rangle$ of $\hat{H}_0$ becomes

$$(E_b - E_a)\,\langle a|-e\hat{\vec{r}}|b\rangle = \frac{-ie\hbar}{m_e}\,\langle a|\hat{\vec{p}}|b\rangle + \left\langle a \middle| \left[-e\hat{\vec{r}}, \hat{V}^{\text{nl}}\right] \middle| b \right\rangle. \tag{36}$$

E_a and E_b are the electronic energies belonging to states $|a\rangle$ and $|b\rangle$. Eq. (36) gives essentially the relation between length and velocity representations of the PtP-polarizability. For more details in a RT-TDDFT framework see Refs.[67,68]

3 Computational details

For all calculations a modified development version of the CP2K[73] package was employed, which includes massively parallelized AIMD[74,75] and RT-TDDFT[76] implementations. As model system a cubic box of liquid S-methyloxirane containing 20 molecules was equilibrated and a production run was performed for 20 ps at a time step of 0.5 fs, which was previously used by one of the authors for the description of NR scattering for periodic systems[46] based on DFPT. The BLYP exchange-correlation functional[77,78] and the TZVP-GTH Gaussian-type pseudo potential basis set[79] were used. Grimme's DFT-D3 dispersion correction[80] was used throughout. 3000 of the AIMD trajectory snapshots at a spacing of 5 fs were used to perform RT-TDDFT calculations on, corresponding to 12.5 ps of signal in total.
For the RT-TDDFT runs the same functional and the DZVP-GTH basis[79] set were used in order to reduce the computational cost. The RT-TDDFT calculations were run at a time step of 0.2 a.u. for at least 20000 steps. As propagator the enforced time reversible symmetry algorithm was used and the matrix exponential was approximated by an Arnoldi subspace algorithm. The ad-hoc finite life time $1/\Gamma$ was chosen to be 0.0037 a.u. = 0.1 eV, consistent with literature.[36] For the calculation of the Fourier transform of the auto correlation functions also a small damping factor was introduced for convergence reasons and in order to reduce noise.

The spectra in the harmonic approximation were artificially broadened by Lorentzians with a full width at half maximum of 20 cm^{-1}.

All Raman spectra are calculated for an experimental set up as described by Eq. (15), if not mentioned otherwise.

The δ-pulse perturbation for the RT-TDDFT runs was applied in the velocity representation as sketched in Ref.[67] using DFPT. During the propagation both the electric dipole moment using the Berry-phase formula in Eq. (33) and the velocity operator including the non-local commutator term as described in Sec. 2.1.2 were tracked, allowing to calculate the PtP-polarizability in the two ways presented above.

The Fourier transforms to obtain the PtP polarizability in the post-processing were performed using Padé approximants in order to reduce the amount of signal required and achieve a continuous frequency resolution.[81] For the post-processing a python tool called 'RTAna' was extended which we used in previous work.[37,67,68]

4 Results

This section is organized as follows: First, the absorption spectra in the gas and liquid phase of (S)-methyloxirane are shown in Sec. 4.1, then gas phase Raman spectra in the double harmonic approximation are given in Sec. 4.2 along with a qualitative analysis of the RR spectra. The results of the dynamic approach are presented in Sec. 4.3 according to the following order: At first the NR scattering cross sections are given in Sec 4.3.1 for both ways of calculating the PtP polarizability in a periodic simulation cell: Using the Berry phase formula and the velocity representation. In Sec. 4.3.2 these two ways are compared for calculating the RR scattering cross section. At last, both NR and RR scattering cross sections of the liquid system are compared to the gas phase harmonic approximation in Sec. 4.4.

4.1 Absorption spectra

The UV/VIS absorption spectrum of a geometry-optimized (S)-methyloxirane molecule is shown in Fig. 1a. The first three excitations are predicted to have excitation energies of 7.42 eV, 7.84 eV and 8.82 eV, respectively.

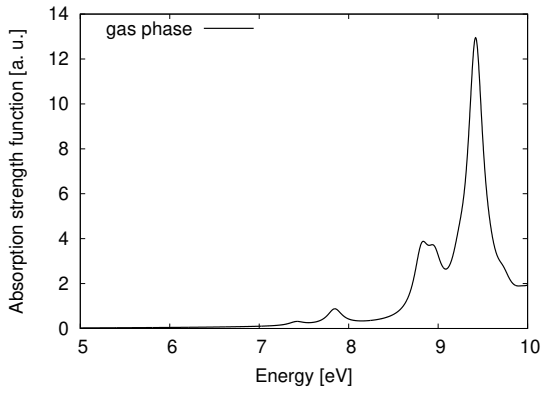

(a) RT-TDDFT absorption spectrum of (S)-methyloxirane (DZVP-GTH/BLYP/D3).

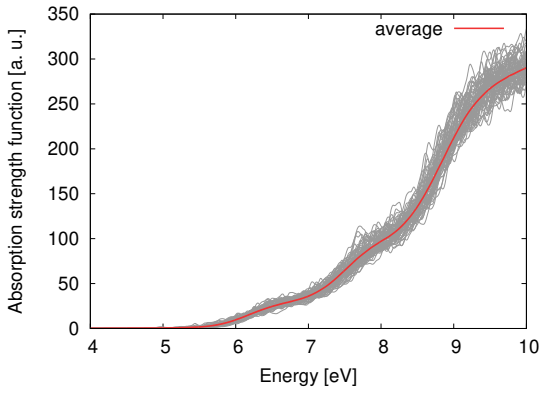

(b) Absorption spectra of 58 different liquid (S)-methyloxirane AIMD frames.

In comparison an ensemble of absorption spectra from individual frames of the AIMD trajectory of liquid (S)-methyloxirane is shown in Fig. 1b and their average is depicted in

red. The life time in Eq. (10) was set to 0.04 eV for the calculations of the absorption spectra on each AIMD frame in order to resolve the finer details in the respective absorption spectra. Here the classical phase space picture of the nuclear motion becomes apparent: Depending on the phase space configuration of the nuclei the (electronic) PtP tensor is different. While sampling this phase space the dynamic approach includes finite temperature effects.

4.2 Double harmonic approximation (gas phase)

The calculation of (resonant) Raman spectra in the double harmonic approximation with RT-TDDFT follows the procedure sketched in Refs.,[36,37,68] using Eq. (14) and the same parameters as for the RT-TDDFT calculations in the dynamic approach. Resulting NR and RR spectra are shown in Fig. 2 where for the RR spectrum the first three excitations at 7.42 eV, 7.84 eV and 8.82 eV were chosen. The RR spectrum shows the characteristic enhancement of the Raman signal by a few orders of magnitude compared to the NR spectrum. Due to the resonance Raman effect the relative intensities of the peaks change as well compared to the NR spectrum according to the (here, short time) wave packet dynamics on the excited state BO surface (Eq. (7)). Most prominently the peak at 722 cm^{-1} is enhanced.

Applying the theory developed by Heller and coworkers[13] leads to rules concerning the relative peak shapes of RR spectra.[82] Important parameters are the displacement of the excited state BO surface w. r. t. the ground state normal modes, as well as the damping factor Γ in Eq. (7). If the molecule shows strong damping, usually the STA is a good approximation. The relative enhancement of peaks in the Raman spectrum are related in a rather complicated way to these changes.[82] Experimentally, relations between the excited state geometry and an enhancement of peaks at normal modes strongly featured in the excited state geometry change have been established.[83]

In this work we use a more qualitative approach: In order to gain insight into why the peak at 722 cm^{-1} is enhanced at the first excitation, an analysis of molecular orbitals contributing to this excitation was carried out following the work by Bruner et al.[81] This

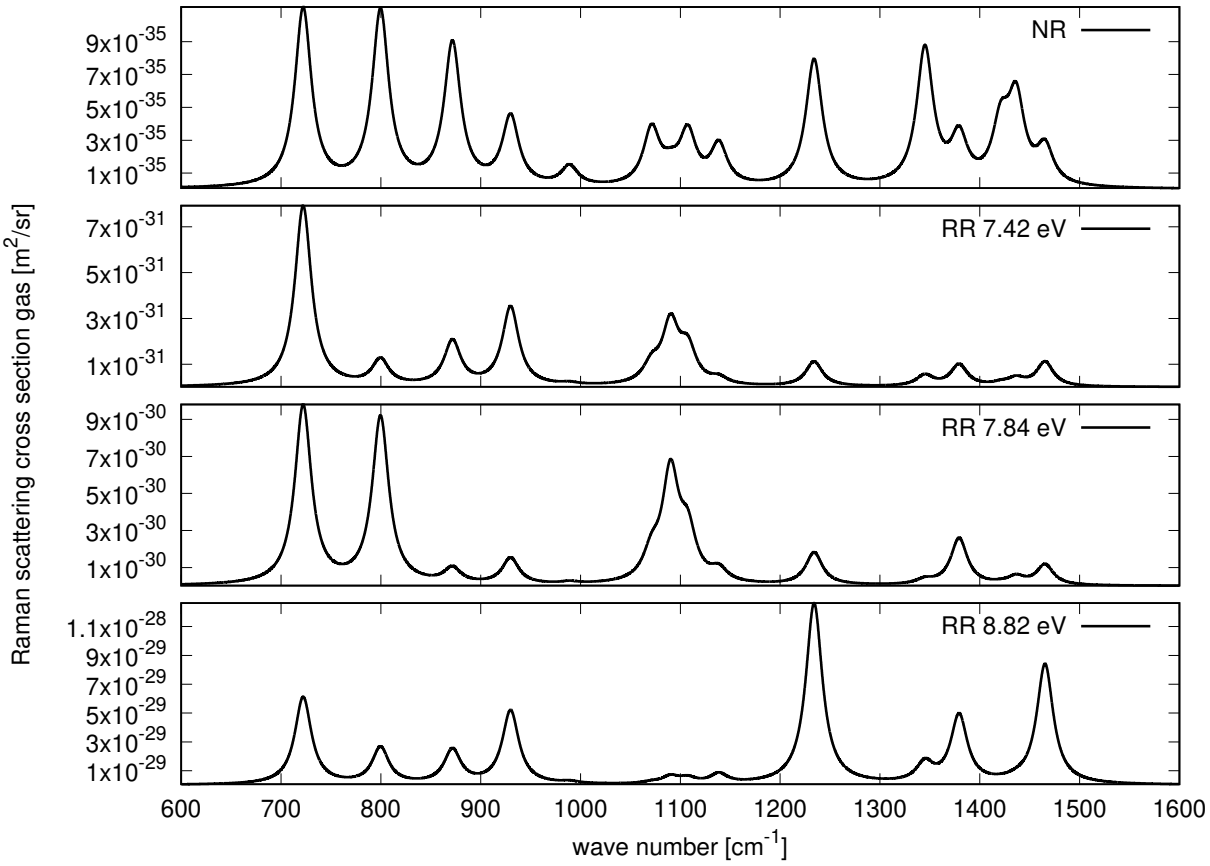

Figure 2: NR and RR scattering cross sections for gas phase (S)-methyloxirane in the double harmonic approximation.

technique allows to obtain a measure for the different contributions of individual occupied-to-virtual molecular orbital transitions to a certain excitation from an RT-TDDFT run, giving results comparable to the amplitudes obtained from a linear response (LR-)TDDFT calculation.[81] The resulting contributions for (S)-methyloxirane in the gas phase are listed in Tab. 1.

From the inspection of the values it is apparent that occupied-virtual transitions starting from the HOMO (MO no. 12) contribute significantly to the first two excitations but less so to the third. The HOMO is mostly comprised of a p-like orbital on the oxygen atom (see Fig. 3b).

The motion of the normal mode corresponding to the peak at 722 cm^{-1} is shown in Fig. 3a. It is a rather complex mode mostly involving a stretching motion between the

Table 1: Contributions of individual occupied-virtual transitions for the first three excited states. The HOMO is labeled as 12.

exc. at 7.42 eV		exc. at 7.84 eV		exc. at 8.82 eV	
transition	contrib.	transition	contrib.	transition	contrib.
12-13	0.67	12-14	0.57	11-13	0.37
12-14	0.33	12-13	0.23	11-14	0.24
		12-15	0.20	10-13	0.14
				12-18	0.07
				9-13	0.06
				12-20	0.05
				12-16	0.04
				10-19	0.02

oxygen atom and the carbon atom at the chiral center. Out of all normal modes this one involves the oxygen atom most strongly. Consequently one might expect a significant excited

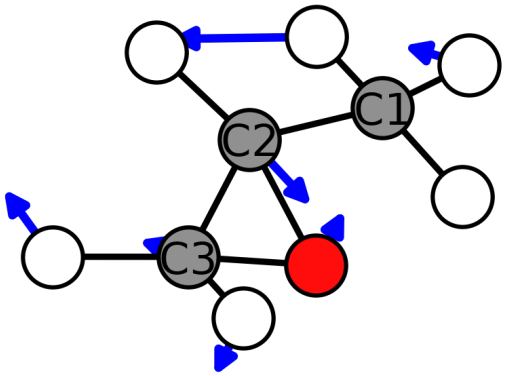

(a) Visualization of normal mode at 722 cm^{-1}.

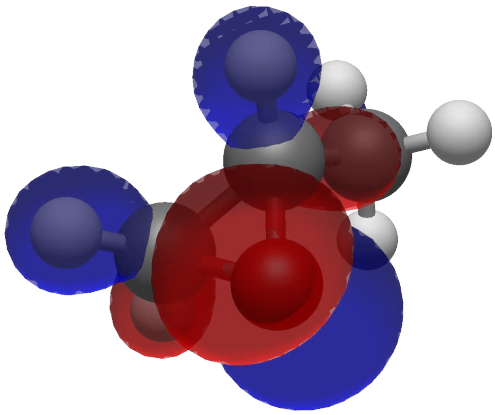

(b) HOMO of (S)-methyloxirane.

state geometry change along the 722 cm^{-1} normal mode for resonances which involve large HOMO contributions, which in turn under specific circumstances would lead to a relative enhancement of that peak in the RR spectrum.

In order to support this the RR spectra at the second and third excitation, at 7.84 eV and 8.82 eV respectively are shown in Fig. 2. Indeed, the RR spectrum at the third excitation at 8.82 eV does not show a strongly enhanced 722 cm^{-1} peak. It does not involve a significant contribution from an occupied-virtual transition starting from the HOMO (see Tab. 1) and

thus its excited state geometry likely does not have a significant displacement along that mode.

We would like to mention that we observed a rather distinct dependence on the computational settings (basis-set, exchange–correlation functional) used in our previous RR calculations with RT-TDDFT in the static harmonic approach.[37,68] Unfortunately we are not aware of any published experimental RR spectrum of (S)-methyloxirane which we could compare to.

4.3 Dynamic approach

4.3.1 Liquid: Non resonant case

The NR scattering cross sections for both the Berry phase and the velocity representation version of the PtP-polarizability are shown in Fig. 4. Apart from minor deviations both the Berry phase formulation and the velocity representation agree very well and appear to be equally suited to describe the polarizability within PBC and the computational settings used.

In Fig. 5 the depolarized NR-scattering cross sections are shown in comparison to the AIMD results obtained from DFPT presented in Ref.[46] by one of the authors and to the experimental spectrum obtained by Polavavapu et al.[84] The particular data used here can be found in the SI of Ref.,[46] corresponding to an AIMD trajectory with the TZVP-GTH basis set and the DFPT calculations for the polarizability with the DZVP-GTH basis set. Both approaches agree reasonably well considering that the DFPT approach was performed in the static limit ($\omega \to 0$) whereas the NR laser frequency here was set to 1.3 eV ($\approx$ 954 nm).

Compared to the experiment a slight deviation of the normal mode frequencies is observed. This can be alleviated by choosing e. g. another basis set or exchange–correlation functional. Hybrid or meta-GGA functionals might be more suited to describe (resonance) Raman scattering and possibly improve the agreement with the experiment. However, the

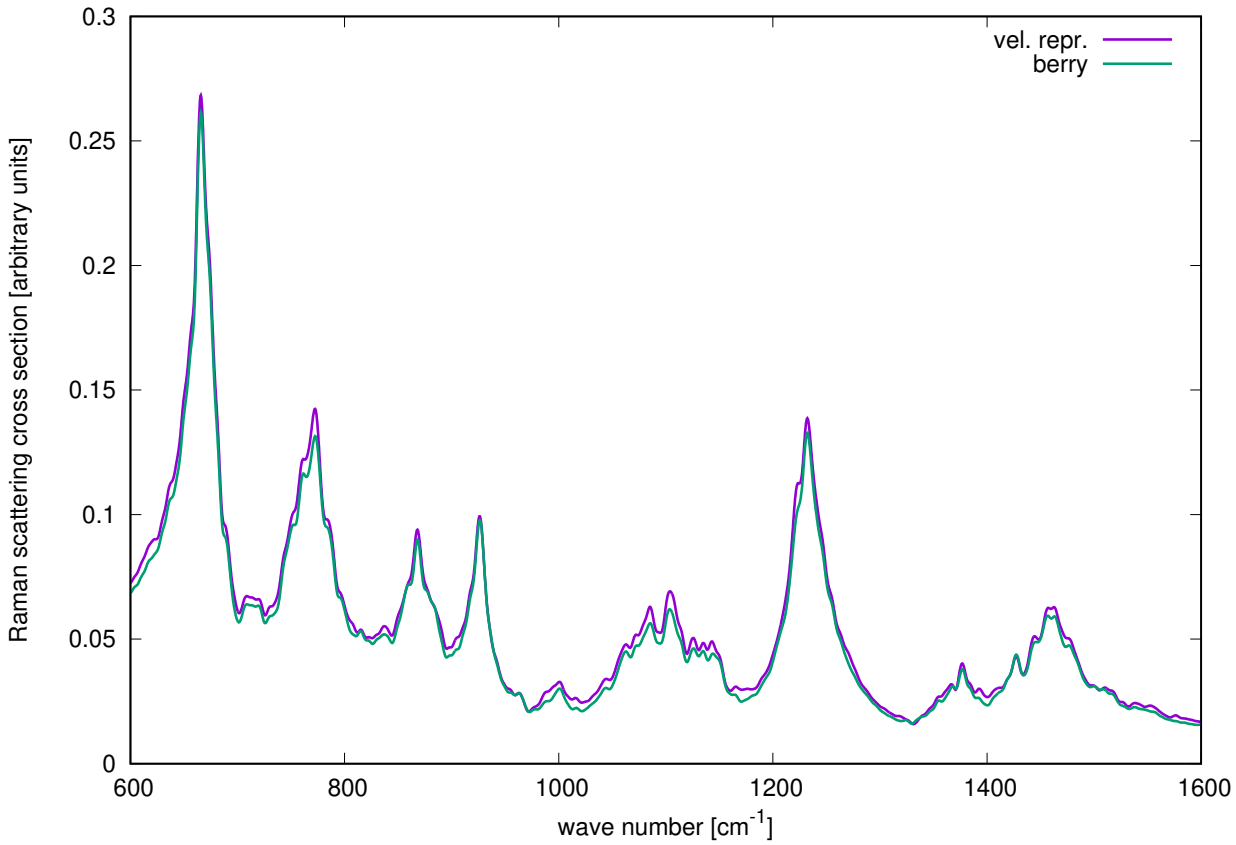

Figure 4: NR scattering cross section for liquid (S)-methyloxirane. The PtP-polarizability was calculated using the Berry phase formula (green) and the velocity representation (purple).

computational cost of applying such a functional is prohibitive at the moment.

As already observed in Ref.[46] 12.5 ps of AIMD signal appear to be enough for a sufficient sampling of the vibrational motion.[46] Characteristically for the dynamic description the peaks are broadened naturally.

In the next section the resonant case is presented, which is available from the same set of simulations owing to the fact that the whole frequency dependent PtP polarizability was obtained via an Fourier transform according to Eqs. (31) and (32).

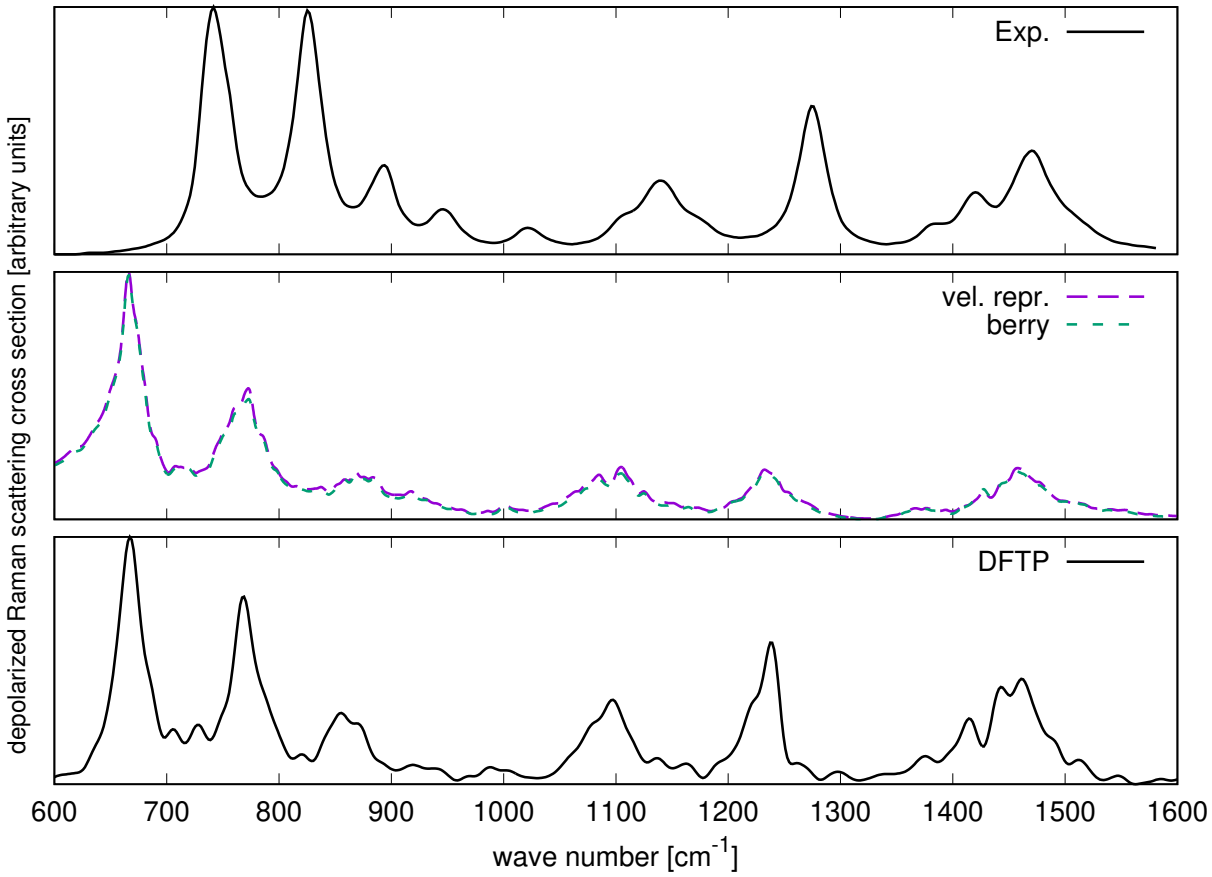

Figure 5: Depolarized NR scattering cross section of liquid (S)-methyloxirane. In the top panel the experimental spectrum given in Ref.[84] was reproduced. The middle panel shows the results of AIMD + RT-TDDFT approach presented in this work, using either the velocity representation or the Berry phase formulation to calculate the polarizability. A previous AIMD result of one of the authors (see. Ref.[46]) using DFPT is shown in the bottom panel.

4.3.2 Liquid: Resonant case

For the presentation of an example of the resonance Raman scattering cross sections, the excitation energy was set to 7.4 eV closely to the first excitation of the gas phase molecule.

This choice is somewhat arbitrary as from the averaged absorption spectra in Fig. 1b it is apparent that the dynamic approach for the liquid does not identify single excitations as in the gas phase, but is rather a blend of all the different phase space configurations.

The RR scattering cross sections are shown in Fig. 6 for both the Berry phase and the velocity representation version of the PtP-polarizability. Again, both formulations agree very well. Since we are not aware of any experimental RR spectrum for (S)-methyloxirane we do

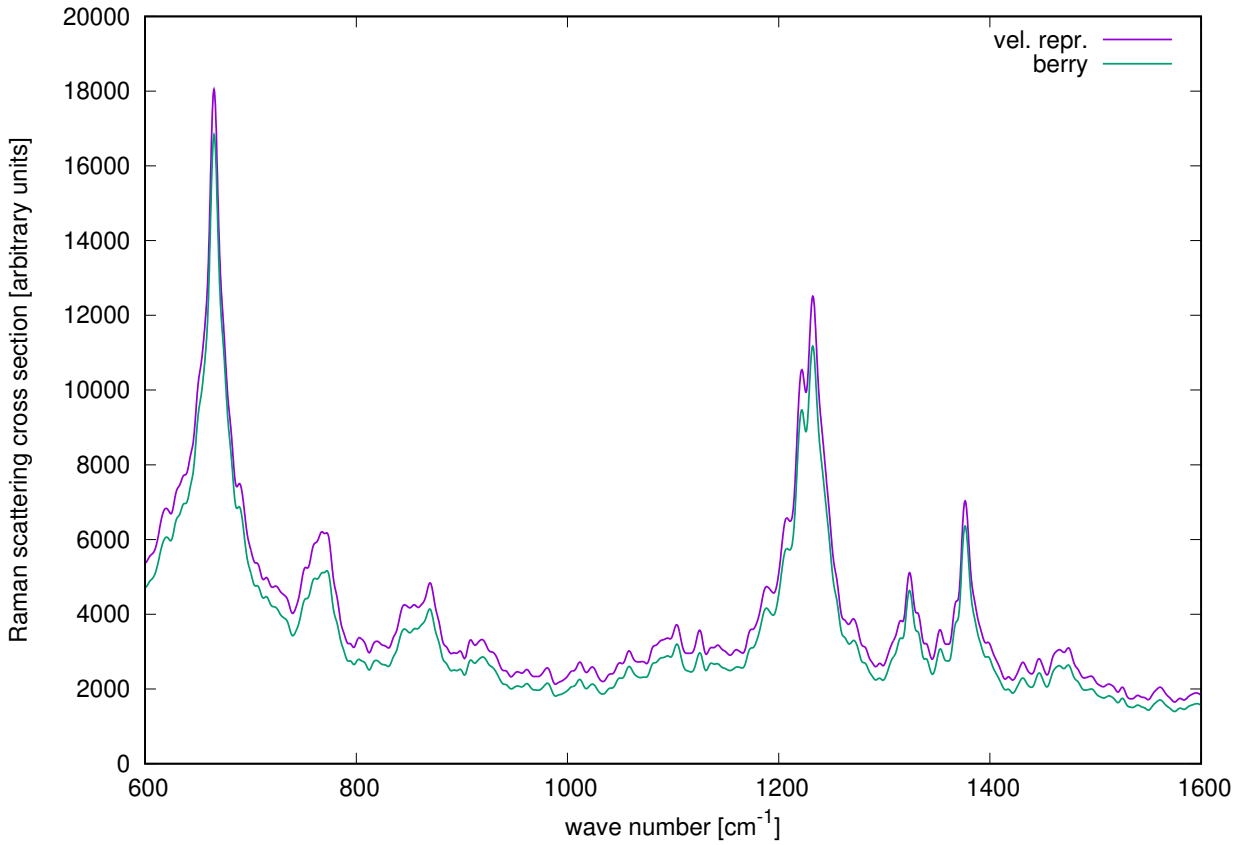

Figure 6: Resonant Raman scattering cross section for liquid (S)-methyloxirane at an excitation energy of 7.4 eV. The PtP-polarizability was calculated using the Berry phase formula (green) and the velocity representation (purple).

not show a comparison to experiment here. Compared to the NR case the RR scattering cross section is several orders of magnitude larger. The fingerprint region of the spectrum shows different relative intensities compared to the NR case due to the averaged (short time) dynamics at the Franck–Condon point of the involved excited state potential energy surfaces at the excitation frequency.

A detailed comparison of the gas phase and the liquid phase Raman spectra is given in the next Section.

4.4 Comparison between double harmonic approximation and dynamic approach

As both the Berry phase and the velocity representation formulations agree very well, here only the Berry phase results are shown.

The NR and RR spectra of the liquid phase, calculated with the AIMD + RT-TDDFT approach are presented in Fig. 7 in comparison to the gas phase spectra obtained in the double harmonic approximation from Sec. 4.2.

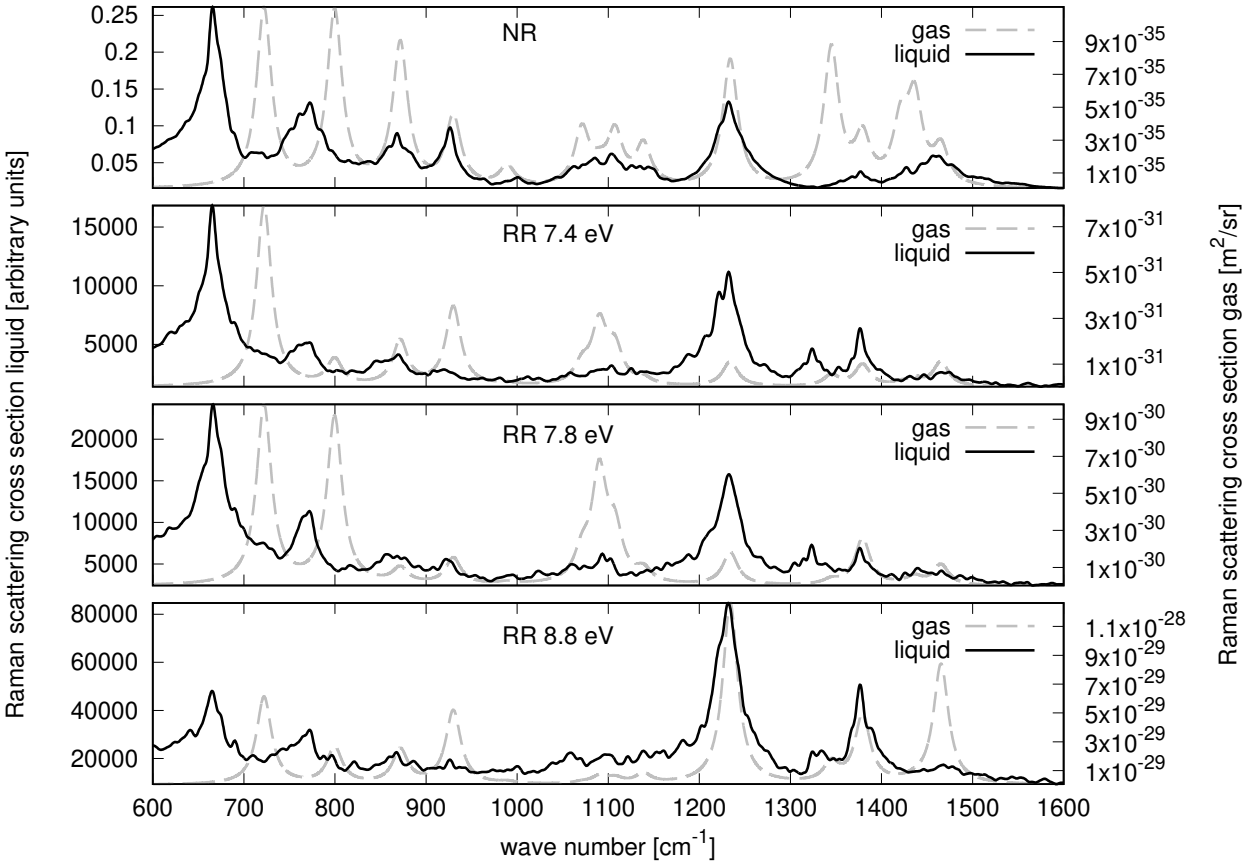

Figure 7: NR and RR scattering cross section for liquid (S)-methyloxirane at different excitation energies using the AIMD+RT-TDDFT approach (black) compared to the double harmonic approximation (gray).

At first we will focus on the NR spectrum. Apart from the natural broadening of the peaks in the dynamic approach due to finite temperature effects we also observe that some of the frequencies in the liquid are shifted. This affects mostly the peaks at 722 cm^{-1}

and 799 cm^{-1} (in the gas phase/harmonic approximation spectrum) which are shifted to lower energies by roughly 50 cm^{-1}. Both of these normal modes are primarily comprised of stretching motions involving the oxygen atom thus indicating a weakened force constant for the oxygen stretching motion due to solvent interactions.[85]

For additional analysis we include the Fourier transforms of the velocity autocorrelation functions of the nuclei in Fig. 8, i. e. the power spectra, which would correspond to the vibrational density of states (VDOS) in the harmonic approximation.[86] The peaks which are shifted the most, namely the gas phase 722 cm^{-1} and 799 cm^{-1} peaks, involve both a high VDOS of the oxygen atom. This is consistent with chemical intuition as the partial charge of the oxygen atom actually leads to stronger solvent interactions and therefore to a weakened force constant. In contrast, the normal mode at 1234 cm^{-1} is very little affected by the change to the liquid phase as it mostly involves core C−C−C stretching/bending which is less prone to solvation effects. This finding is supported by the VDOS as well.

The relative intensities of the peaks also change between gas and liquid phase; especially the features above 1300 cm^{-1} appear at different wave numbers and show different relative intensities.

In the resonant case the differences between the gas phase and liquid spectra are more pronounced. In the RR spectrum of the liquid at an excitation energy of 7.4 eV presented in Fig. 7 only two peaks at 650 cm^{-1} and 1234 cm^{-1} are prominent whereas other peaks appear generally broadened and less intense. The features in the gas phase spectrum around 1100 cm^{-1} are barely emerging above the noise level while the peak at around 1234 cm^{-1} is more prominent in the liquid spectrum than in the gas phase.

Although the character of the MOs is more complex and de-localized in the liquid the relative enhancement of the peaks is still comparable to that discussed for the gas phase spectrum in Sec. 4.2. Thus in the transition from a single gas phase molecule to the phase space sampling of the liquid some features of the RR spectrum carry over: The gas phase 722 cm^{-1} peak which appears at 650 cm^{-1} in the liquid is still most prominent.

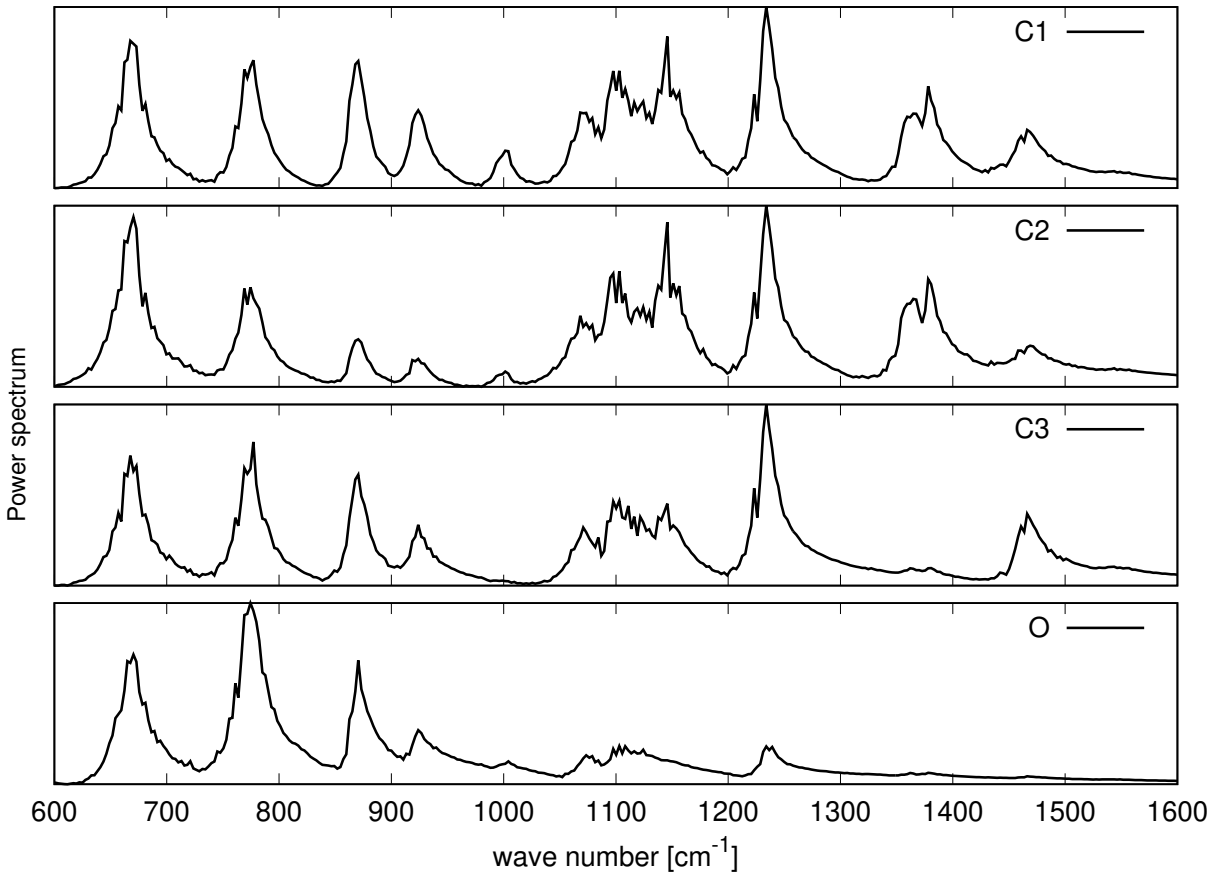

Figure 8: Power spectra of the individual atoms of (S)-methyloxirane during the AIMD. The labeling of the C atoms is given in Fig. 3a.

The peak at 929 cm^{-1} which is clearly visible in the gas phase and liquid NR spectra vanishes almost entirely in the (liquid) resonance case. This may partially be explained by this mode being a tilting motion of the CH_3 group which may be hindered due to solvation effects. The fact that this is most evident for the RR spectrum at an excitation energy of 7.4 eV points to the electronic structure playing a significant role. Unfortunately information about the individual electronic transitions involved at that energy range in the liquid are hard to extract as in RT-TDDFT (and using a delta pulse) all electronic states are propagated simultaneously. Additionally the high density of electronic states in the liquid phase makes an analysis as in Sec. 4.2 difficult from a numerical point of view.

Considering also two other RR spectra at 7.8 eV and 8.8 eV respectively in Fig. 7 a similar picture emerges: Some peaks of the liquid spectrum are very similar as in the gas

phase spectrum e. g. the 1234 cm^{-1} peak at an excitation energy of 8.8 eV while others show enhancement/de-enhancement compared to the gas phase spectrum.

In the liquid many close lying excited states contribute at a certain excitation energy and in the dynamic approach presented here these various contributions are sampled for different phase space configurations of the nuclear classical phase space. An indication of this averaged picture is that the 1234 cm^{-1} peak, which is barely relevant in the gas phase RR spectra of the first two excited electronic states grows into prominence in the liquid already at an excitation energy of 7.4 eV until it reaches its maximum at 8.8 eV.

4.5 Excitation profile

The great advantage of RT-TDDFT is that the whole excitation profile can be obtained, as the whole frequency dependent electric-dipole–electric-dipole polarizability tensor is available via the FT. This is illustrated in the excitation profile of liquid (S)-methyloxirane in Fig. 9.

Apart from the resonance effect covering roughly 5 orders of magnitude, also a pre-resonant enhancement of the Raman signal is visible. The emergence of the enhanced 1234 cm^{-1} peak as seen in Fig. 7 can be followed easily in the profile.

Compared to the excitation profile in the harmonic approximation previously published in Ref.[37] the broadening of the peaks due to the dynamic approach is clearly visible and manifests itself in an upward slope as the resonance regime is approached.

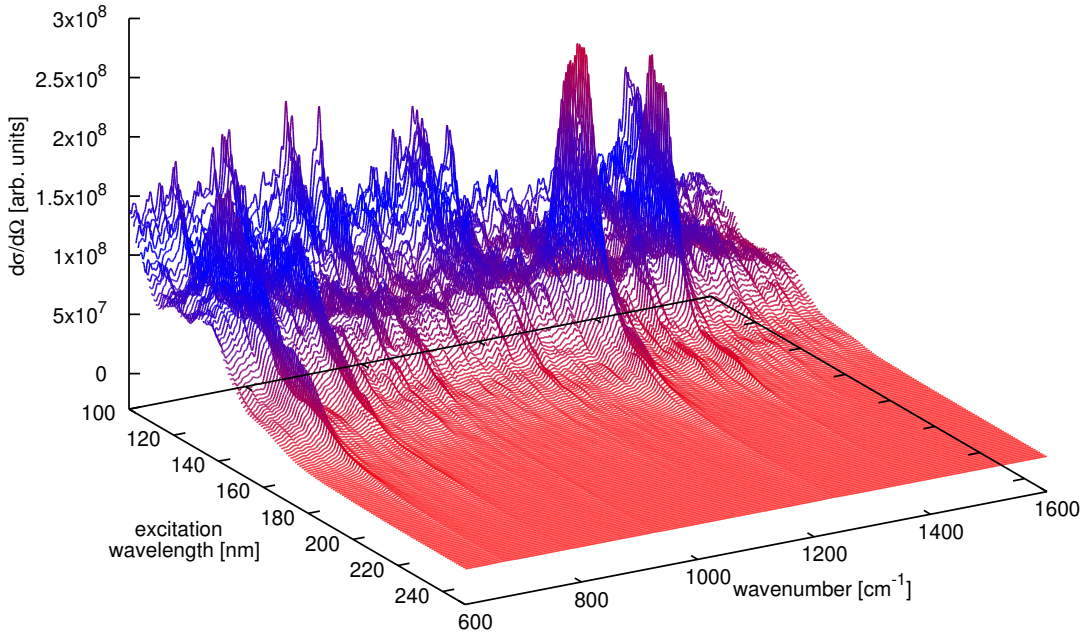

Figure 9: Raman excitation profile of liquid (S)-methyloxirane.

5 Conclusion

In this work a comprehensive discussion of the theoretical derivation of a dynamic approach to calculate non-resonant as well as (near-) resonant Raman spectra in the condensed phase was given. The methodology consists of the combination of AIMD with RT-TDDFT. In the non-resonant case it reduces to Plazcek's theory for Raman scattering whereas in (pre-)resonant case it corresponds to a short time approximation of Heller's time dependent formulation of Raman scattering, essentially using a Plazcek-type polarizability.[54]
Combining these two dynamic methods gives the advantages of both: AIMD provides a treatment of molecular vibrations beyond the harmonic approximation and the inclusion of finite temperature effects as well as a description of system and environment on the same level of theory using periodic boundary conditions. RT-TDDFT allows the calculation of the whole frequency dependent electronic polarizability at once via Fourier transforms in an efficient manner. The intricacies of defining the polarization in a periodic system are discussed and two approaches were used:

1. Using the modern theory of polarization based on the Berry phase.

2. Using the velocity representation of the electric-dipole–electric-dipole polarizability.

For a system of liquid (S)-methyloxirane both of these formulations are compared and found to be in very good agreement in the non-resonant as well as in the resonant case for the computational settings used.

Additionally an extensive comparison between the gas phase / double harmonic approximation and the dynamic approach is given considering absorption as well as non-resonant and (near-) resonant Raman spectra, highlighting the treatment of finite temperature effects and the interactions in the liquid phase.

Despite its high cost compared to the harmonic approximation this methodology is promising for the modeling of non-resonant as well as (near-) resonant Raman spectra of complex, condensed phase systems as it can provide an explicit dynamic treatment of the

system under study as well as an efficient, although approximate, calculation of resonance Raman scattering cross sections for the whole range of excitation frequencies.

6 Acknowledgements

This work has been supported by the University of Zurich, the university Research Priority Program "Solar Light to Chemical Energy Conversion" (LightChEC), and the Swiss National Foundation (grant no. PP00P2_170667). Our calculations have been supported by the Swiss National Supercomputing Center, accounts s745, s788, and s875.

References

(1) Rygula, A.; Majzner, K.; Marzec, K. M.; Kaczor, A.; Pilarczyk, M.; Baranska, M. Raman spectroscopy of proteins: a review. *J. Raman Spectrosc.* **2013**, *44*, 1061–1076.

(2) Czamara, K.; Majzner, K.; Pacia, M. Z.; Kochan, K.; Kaczor, A.; Baranska, M. Raman spectroscopy of lipids: a review. *J. Raman Spectrosc.* **2015**, *46*, 4–20.

(3) Malard, L.; Pimenta, M.; Dresselhaus, G.; Dresselhaus, M. Raman spectroscopy in graphene. *Phys. Rep.* **2009**, *473*, 51 – 87.

(4) Dresselhaus, M.; Dresselhaus, G.; Saito, R.; Jorio, A. Raman spectroscopy of carbon nanotubes. *Phys. Rep.* **2005**, *409*, 47 – 99.

(5) Tolles, W. M.; Nibler, J. W.; McDonald, J. R.; Harvey, A. B. A Review of the Theory and Application of Coherent Anti-Stokes Raman Spectroscopy (CARS). *Appl. Spectrosc.* **1977**, *31*, 253–271.

(6) McNay, G.; Eustace, D.; Smith, W. E.; Faulds, K.; Graham, D. Surface-Enhanced Raman Scattering (SERS) and Surface-Enhanced Resonance Raman Scattering (SERRS): A Review of Applications. *Appl. Spectrosc.* **2011**, *65*, 825–837.

(7) Stiles, P. L.; Dieringer, J. A.; Shah, N. C.; Van Duyne, R. P. Surface-Enhanced Raman Spectroscopy. *Annu. Rev. Anal. Chem.* **2008**, *1*, 601–626.

(8) Schmid, T.; Opilik, L.; Blum, C.; Zenobi, R. Nanoscale Chemical Imaging Using Tip-Enhanced Raman Spectroscopy: A Critical Review. *Angew. Chem.* **2013**, *52*, 5940–5954.

(9) Kramers, H. A.; Heisenberg, W. Über die Streuung von Strahlung durch Atome. *Zeitschrift für Physik* **1925**, *31*, 681–708.

(10) Dirac, P. A. M.; Fowler, R. H. The quantum theory of dispersion. *Proc. Roy. Soc. A* **1927**, *114*, 710–728.

(11) Dirac, P. A. M.; Bohr, N. H. D. The quantum theory of the emission and absorption of radiation. *Proc. Roy. Soc. A* **1927**, *114*, 243–265.

(12) Albrecht, A. C. On the Theory of Raman Intensities. *J. Chem. Phys.* **1961**, *34*, 1476–1484.

(13) Lee, S.; Heller, E. J. Timedependent theory of Raman scattering. *J. Chem. Phys.* **1979**, *71*, 4777–4788.

(14) Heller, E. J.; Sundberg, R.; Tannor, D. Simple aspects of Raman scattering. *J. Phys. Chem.* **1982**, *86*, 1822–1833.

(15) Kane, K. A.; Jensen, L. Calculation of Absolute Resonance Raman Intensities: Vibronic Theory vs Short-Time Approximation. *J. Phys. Chem. C* **2010**, *114*, 5540–5546.

(16) Champion, P. M.; Albrecht, A. C. Resonance Raman Scattering: The Multimode Problem and Transform Methods. *Annu. Rev. Phys. Chem.* **1982**, *33*, 353–376.

(17) Peticolas, W. L.; Rush III, T. Ab initio calculations of the ultraviolet resonance Raman spectra of uracil. *J. Comput. Chem.* **1995**, *16*, 1261–1270.

(18) Romanova, J.; Ligeois, V.; Champagne, B. Resonant Raman spectra of molecules with diradical character: multiconfigurational wavefunction investigation of neutral viologens. *Phys. Chem. Chem. Phys.* **2014**, *16*, 21721–21731.

(19) Guthmuller, J.; Champagne, B. Time dependent density functional theory investigation of the resonance Raman properties of the julolidinemalononitrile push-pull chromophore in various solvents. *J. Chem. Phys.* **2007**, *127*, 164507.

(20) Guthmuller, J.; Champagne, B. Resonance Raman Spectra and Raman Excitation Profiles of Rhodamine 6G from Time-Dependent Density Functional Theory. *ChemPhysChem* **2008**, *9*, 1667–1669.

(21) Baiardi, A.; Bloino, J.; Barone, V. A general time-dependent route to Resonance-Raman spectroscopy including Franck-Condon, Herzberg-Teller and Duschinsky effects. *J. Chem. Phys.* **2014**, *141*, 114108.

(22) Jensen, L.; Zhao, L. L.; Autschbach, J.; Schatz, G. C. Theory and method for calculating resonance Raman scattering from resonance polarizability derivatives. *J. Chem. Phys.* **2005**, *123*, 174110.

(23) Jensen, L.; Schatz, G. C. Resonance Raman Scattering of Rhodamine 6G as Calculated Using Time-Dependent Density Functional Theory. *J. Phys. Chem. A* **2006**, *110*, 5973–5977.

(24) Kupfer, S.; Wächtler, M.; Guthmuller, J.; Popp, J.; Dietzek, B.; González, L. A Novel Ru(II) Polypyridine Black Dye Investigated by Resonance Raman Spectroscopy and TDDFT Calculations. *J. Phys. Chem. C* **2012**, *116*, 19968–19977.

(25) Zedler, L.; Guthmuller, J.; Rabelo de Moraes, I.; Kupfer, S.; Krieck, S.; Schmitt, M.; Popp, J.; Rau, S.; Dietzek, B. Resonance-Raman spectro-electrochemistry of intermediates in molecular artificial photosynthesis of bimetallic complexes. *Chem. Commun.* **2014**, *50*, 5227–5229.

(26) Herrmann, C.; Neugebauer, J.; Presselt, M.; Uhlemann, U.; Schmitt, M.; Rau, S.; Popp, J.; Reiher, M. The First Photoexcitation Step of Ruthenium-Based Models for Artificial Photosynthesis Highlighted by Resonance Raman Spectroscopy. *J. Phys. Chem. B* **2007**, *111*, 6078–6087.

(27) Guthmuller, J.; Champagne, B.; Moucheron, C.; Kirsch De Mesmaeker, A. Investigation of the Resonance Raman Spectra and Excitation Profiles of a Monometallic Ruthenium(II) [Ru(bpy)2(HAT)]2+ Complex by Time-Dependent Density Functional Theory. *J. Phys. Chem. B* **2010**, *114*, 511–520.

(28) Guthmuller, J.; González, L. Simulation of the resonance Raman intensities of a ruthenium-palladium photocatalyst by time dependent density functional theory. *Phys. Chem. Chem. Phys.* **2010**, *12*, 14812–14821.

(29) Mullin, J. M.; Autschbach, J.; Schatz, G. C. Time-dependent density functional methods for surface enhanced Raman scattering (SERS) studies. *Comput. Theor. Chem.* **2012**, *987*, 32 – 41.

(30) Aikens, C. M.; Schatz, G. C. TDDFT Studies of Absorption and SERS Spectra of Pyridine Interacting with Au20. *J. Phys. Chem. A* **2006**, *110*, 13317–13324.

(31) Silverstein, D. W.; Govind, N.; van Dam, H. J. J.; Jensen, L. Simulating One-Photon Absorption and Resonance Raman Scattering Spectra Using Analytical Excited State Energy Gradients within Time-Dependent Density Functional Theory. *J. Chem. Theory Comput.* **2013**, *9*, 5490–5503.

(32) Tschirner, N.; Schenderlein, M.; Brose, K.; Schlodder, E.; Mroginski, M. A.; Thomsen, C.; Hildebrandt, P. Resonance Raman spectra of -carotene in solution and in photosystems revisited: an experimental and theoretical study. *Phys. Chem. Chem. Phys.* **2009**, *11*, 11471–11478.

(33) Wilson, E. B.; Decius, J. C.; Cross, P. C. *Molecular Vibrations: The Theory of Infrared and Raman Vibrational Spectra*; DOVER PUBN INC, 1980.

(34) Luber, S.; Reiher, M. Intensity-Carrying Modes in Raman and Raman Optical Activity Spectroscopy. *ChemPhysChem* **2009**, *10*, 2049–2057.

(35) Cornaton, Y.; Ringholm, M.; Louant, O.; Ruud, K. Analytic calculations of anharmonic infrared and Raman vibrational spectra. *Phys. Chem. Chem. Phys.* **2016**, *18*, 4201–4215.

(36) Thomas, M.; Latorre, F.; Marquetand, P. Resonance Raman spectra of ortho-nitrophenol calculated by real-time time-dependent density functional theory. *J. Chem. Phys.* **2013**, *138*, 044101.

(37) Mattiat, J.; Luber, S. Efficient calculation of (resonance) Raman spectra and excitation profiles with real-time propagation. *J. Chem. Phys.* **2018**, *149*, 174108.

(38) Corni, S.; Cappelli, C.; Cammi, R.; Tomasi, J. Theoretical Approach to the Calculation of Vibrational Raman Spectra in Solution within the Polarizable Continuum Model. *J. Phys. Chem. A* **2001**, *105*, 8310–8316.

(39) Mennucci, B.; Cappelli, C.; Cammi, R.; Tomasi, J. A quantum mechanical polarizable continuum model for the calculation of resonance Raman spectra in condensed phase. *Theor. Chem. Acc.* **2007**, *117*, 1029–1039.

(40) Sezer, M.; Woelke, A.-L.; Knapp, E. W.; Schlesinger, R.; Mroginski, M. A.; Weidinger, I. M. Redox induced protonation of heme propionates in cytochrome c oxidase: Insights from surface enhanced resonance Raman spectroscopy and QM/MM calculations. *BBA-Bioenergetics* **2017**, *1858*, 103 – 108.

(41) Kupfer, S.; Zedler, L.; Guthmuller, J.; Bode, S.; Hager, M. D.; Schubert, U. S.; Popp, J.; Grfe, S.; Dietzek, B. Self-healing mechanism of metallopolymers investigated by QM/MM simulations and Raman spectroscopy. *Phys. Chem. Chem. Phys.* **2014**, *16*, 12422–12432.

(42) Apr, E.; Bhattarai, A.; Crampton, K. T.; Bylaska, E. J.; Govind, N.; Hess, W. P.; El-Khoury, P. Z. Time Domain Simulations of Single Molecule Raman Scattering. *J. Phys. Chem. A* **2018**, *122*, 7437–7442.

(43) Ren, H.; Jiang, J.; Mukamel, S. Deep UV Resonance Raman Spectroscopy of -Sheet Amyloid Fibrils: A QM/MM Simulation. *J. Phys. Chem. B* **2011**, *115*, 13955–13962.

(44) GORDON, R. In *Advances in Magnetic Resonance*; WAUGH, J. S., Ed.; Advances in Magnetic and Optical Resonance; Academic Press, 1968; Vol. 3; pp 1 – 42.

(45) Pagliai, M.; Cavazzoni, C.; Cardini, G.; Erbacci, G.; Parrinello, M.; Schettino, V. Anharmonic infrared and Raman spectra in CarParrinello molecular dynamics simulations. *The Journal of Chemical Physics* **2008**, *128*, 224514.

(46) Luber, S.; Iannuzzi, M.; Hutter, J. Raman spectra from ab initio molecular dynamics and its application to liquid S-methyloxirane. *J. Chem. Phys.* **2014**, *141*, 094503.

(47) Thomas, M.; Brehm, M.; Fligg, R.; Vhringer, P.; Kirchner, B. Computing vibrational spectra from ab initio molecular dynamics. *Phys. Chem. Chem. Phys.* **2013**, *15*, 6608–6622.

(48) Brehm, M.; Thomas, M. Computing Bulk Phase Resonance Raman Spectra from ab Initio Molecular Dynamics and Real-Time TDDFT. *J. Chem. Theory Comput.* **2019**, *15*, 3901–3905.

(49) Loudon, R. *The Quantum Theory of Light*, 3rd ed.; Oxford University Press: Great Clarendon Street, Oxford 0x2 6dp, 2000.

(50) Sakurai, J. J. *Advanced Quantum Mechanics*; Addison-Wesley, 1967.

(51) Born, M.; Oppenheimer, R. Zur Quantentheorie der Molekeln. *Annalen der Physik* **1927**, *389*, 457–484.

(52) Tannor, D. J.; Heller, E. J. Polyatomic Raman scattering for general harmonic potentials. *J. Chem. Phys.* **1982**, *77*, 202–218.

(53) Long, D. A. *The Raman Effect*; John Wiley & Sons, Ltd., 2002.

(54) Lee, S. Placzektype polarizability tensors for Raman and resonance Raman scattering. *J. Chem. Phys.* **1983**, *78*, 723–734.

(55) Walter, M.; Moseler, M. Ab Initio Wavelength-Dependent Raman Spectra: Placzek Approximation and Beyond. *J. Chem. Theory Comput.* **2020**, *16*, 576–586.

(56) Neugebauer, J.; Reiher, M.; Kind, C.; Hess, B. A. Quantum chemical calculation of vibrational spectra of large moleculesRaman and IR spectra for Buckminsterfullerene. *J. Comput. Chem.* **2002**, *23*, 895–910.

(57) McQuarrie, D. A. *Statistical Mechanics*; Harper & Row, 1973.

(58) Hecht, L.; Nafie, L. A. Theory of natural Raman optical activity. *Mol. Phys.* **1991**, *72*, 441–469.

(59) Gordon, R. G. Relations between Raman Spectroscopy and Nuclear Spin Relaxation. *J. Chem. Phys.* **1965**, *42*, 3658–3665.

(60) Ramirez, R.; López-Ciudad, T.; Kumar P, P.; Marx, D. Quantum corrections to classical time-correlation functions: Hydrogen bonding and anharmonic floppy modes. *J. Chem. Phys.* **2004**, *121*, 3973–3983.

(61) Yabana, K.; Bertsch, G. F. Time-dependent local-density approximation in real time: Application to conjugated molecules. *Int. J. Quantum. Chem.* **1999**, *75*, 55–66.

(62) Jensen, J.; Mackintosh, A. R. *Rare Earth Magnetism: Structures and Excitations*; Clarendon Press, Oxford, 1991; pp 134–162.

(63) Yabana, K.; Nakatsukasa, T.; Iwata, J. I.; Bertsch, G. F. Real-time, real-space implementation of the linear response time-dependent density-functional theory. *Phys. Status Solidi B* **2006**, *243*, 1121–1138.

(64) Vanderbilt, D. *Berry Phases in Electronic Structure Theory*; Cambridge University Press, 2018.

(65) Resta, R. Quantum-Mechanical Position Operator in Extended Systems. *Phys. Rev. Lett.* **1998**, *80*, 1800–1803.

(66) King-Smith, R. D.; Vanderbilt, D. Theory of polarization of crystalline solids. *Phys. Rev. B* **1993**, *47*, 1651–1654.

(67) Mattiat, J.; Luber, S. Electronic circular dichroism with real time time dependent density functional theory: Propagator formalism and gauge dependence. *Chem. Phys.* **2019**, *527*, 110464.

(68) Mattiat, J.; Luber, S. Vibrational (resonance) Raman optical activity with real time time dependent density functional theory. *J. Chem. Phys.* **2019**, *151*, 234110.

(69) Ismail-Beigi, S.; Chang, E. K.; Louie, S. G. Coupling of nonlocal potentials to electromagnetic fields. *Phys. Rev. Lett.* **2001**, *87*, 87402–1–87402–4.

(70) Pickard, C. J.; Mauri, F. All-electron magnetic response with pseudopotentials: NMR chemical shifts. *Phys. Rev. B* **2001**, *63*, 1–13.

(71) Pickard, C. J.; Mauri, F. Nonlocal pseudopotentials and magnetic fields. *Phys. Rev. Lett.* **2003**, *91*, 7–10.

(72) Varsano, D.; Espinosa-Leal, L. A.; Andrade, X.; Marques, M. A. L.; di Felice, R.; Rubio, A. Towards a gauge invariant method for molecular chiroptical properties in TDDFT. *Phys. Chem. Chem. Phys.* **2009**, *11*, 4481–4489.

(73) CP2K version 7.0 (Developement Version), the CP2K developers group (2019); available from `http://www.cp2k.org`.

(74) Vandevondele, J.; Krack, M.; Mohamed, F.; Parrinello, M.; Chassaing, T.; Hutter, J. Quickstep: Fast and accurate density functional calculations using a mixed Gaussian and plane waves approach. *Comput. Phys. Commun.* **2005**, *167*, 103–128.

(75) Hutter, J.; Iannuzzi, M.; Schiffmann, F.; Vandevondele, J. CP2K: Atomistic simulations of condensed matter systems. *Wiley Interdiscip. Rev. Comput. Mol. Sci.* **2014**, *4*, 15–25.

(76) Andermatt, S.; Cha, J.; Schiffmann, F.; VandeVondele, J. Combining linear-scaling DFT with subsystem DFT in born-oppenheimer and ehrenfest molecular dynamics simulations: From molecules to a virus in solution. *J. Chem. Theory Comput.* **2016**, *12*, 3214–3227.

(77) Becke, A. D. Density-functional exchange-energy approximation with correct asymptotic behavior. *Phys. Rev. A* **1988**, *38*, 3098–3100.

(78) Lee, C.; Yang, W.; Parr, R. G. Development of the Colle-Salvetti correlation-energy formula into a functional of the electron density. *Phys. Rev. B* **1988**, *37*, 785–789.

(79) VandeVondele, J.; Hutter, J. Gaussian basis sets for accurate calculations on molecular systems in gas and condensed phases. *J. Chem. Phys.* **2007**, *127*.

(80) Grimme, S.; Antony, J.; Ehrlich, S.; Krieg, H. A consistent and accurate ab initio parametrization of density functional dispersion correction (DFT-D) for the 94 elements H-Pu. *J. Chem. Phys.* **2010**, *132*, 154104.

(81) Bruner, A.; LaMaster, D.; Lopata, K. Accelerated Broadband Spectra Using Transition Dipole Decomposition and Padé Approximants. *J. Chem. Theory Comput.* **2016**, *12*, 3741–3750.

(82) Shin, K. S. K.; Zink, J. I. Quantitative evaluation of the relationships between excited-state geometry and the intensities of fundamentals, overtones, and combination bands in resonance Raman spectra. *Inorg. Chem.* **1989**, *28*, 4358–4366.

(83) Hirakawa, A. Y.; Tsuboi, M. Molecular Geometry in an Excited Electronic State and a Preresonance Raman Effect. *Science* **1975**, *188*, 359–361.

(84) Polavarapu, P. L.; Hecht, L.; Barron, L. D. Vibrational Raman optical activity in substituted oxiranes. *J. Phys. Chem.* **1993**, *97*, 1793–1799.

(85) Šebestík, J.; Bouř, P. Raman Optical Activity of Methyloxirane Gas and Liquid. *J. Phys. Chem. Lett.* **2011**, *2*, 498–502.

(86) Gonçalves, S.; Bonadeo, H. Vibrational densities of states from molecular-dynamics calculations. *Phys. Rev. B* **1992**, *46*, 12019–12021.

Graphical TOC Entry